

# Earth's Future

## RESEARCH ARTICLE

10.1029/2021EF002016

### Key Points:

- Urban heat
- Climate equity
- Environmental justice

### Supporting Information:

Supporting Information may be found in the online version of this article.

### Correspondence to:

S. A. Benz and J. A. Burney,  
[sabenz@ucsd.edu](mailto:sabenz@ucsd.edu);  
[jburney@ucsd.edu](mailto:jburney@ucsd.edu)



### Citation:

Benz, S. A., & Burney, J. A. (2021). Widespread race and class disparities in surface urban heat extremes across the United States. *Earth's Future*, 9, e2021EF002016. <https://doi.org/10.1029/2021EF002016>

Received 1 FEB 2021  
 Accepted 10 JUN 2021

© 2021. The Authors.  
 This is an open access article under the terms of the [Creative Commons Attribution-NonCommercial License](https://creativecommons.org/licenses/by-nc/4.0/), which permits use, distribution and reproduction in any medium, provided the original work is properly cited and is not used for commercial purposes.

# Widespread Race and Class Disparities in Surface Urban Heat Extremes Across the United States

Susanne Amelie Benz<sup>1</sup>  and Jennifer Anne Burney<sup>1</sup> 

<sup>1</sup>School of Global Policy and Strategy, UC San Diego, La Jolla, CA, USA

**Abstract** Here we use remotely sensed land surface temperature measurements to explore the distribution of the United States' urban heating burden, both at high resolution (within cities or counties) and at scale (across the whole contiguous United States). While a rich literature has documented neighborhood-level disparities in urban heat exposures in individual cities, data constraints have precluded comparisons across locations. Here, drawing on urban temperature anomalies during extreme summer surface temperature events from all 1,056 US counties with more than 10 developed census tracts, we find that the poorest tracts (and those with lowest average education levels) within a county are significantly hotter than the richest (and more educated) neighborhoods for 76% of these counties (54% for education); we also find that neighborhoods with higher Black, Hispanic, and Asian population shares are hotter than the more White, non-Hispanic areas in each county. This holds in counties with both large and small spreads in these population shares, and for 71% of all counties the significant racial urban heat disparities persist even when adjusting for income. Although individual locations have different histories that have contributed to race- and class-based geographies, we find that the physical features of the urban environments driving these surface heat exposure gradients are fairly uniform across the country. Systematically, the disproportionate heat surface exposures faced by minority communities are due to more built-up neighborhoods, less vegetation, and—to a lesser extent—higher population density.

**Plain Language Summary** Particularly in summer, warming in cities due to alterations of the surface energy balance jeopardizes human health and productivity. The distribution of excess urban heat varies within cities, and as a result communities do not share a city's extreme heat burden equally. We find that, within counties across the United States—even with their very different geographies and histories—neighborhoods with lower-income and higher shares of non-white residents experience significantly more extreme surface urban heat than their wealthier, whiter counterparts. Here we quantify these race and class disparities across the United States—they appear in more than 70% of all counties—and show that, while the social, political, and economic drivers of these disparities may differ, the structure of the built environment driving these changes are quite uniform.

## 1. Introduction

Changes in land cover due to urbanization alter the local surface energy balance, often raising city temperatures at the surface, in the subsurface, and in the atmosphere, compared to their rural surroundings (Grimmond, 2007). These average differences can be substantial, and create an added thermal risk for the rapidly urbanizing global population, as extreme heat is detrimental to human health and welfare across a range of metrics (Anderson & Bell, 2009; Hsiang et al., 2013). Yet even *within* cities, temperature anomalies can vary dramatically over short distances as a function of physical neighborhood characteristics. This heterogeneity is not without consequence: particularly during summer heat waves, within-city air temperature differences can delineate life-or-death conditions (e.g., Laaidi et al., 2012; Pyrgou & Santamouris, 2018; Ridder et al., 2016; Taylor et al., 2015; Whitman et al., 1997; J. Yang et al., 2019).

Traditional heat exposure quantities for human health, like wet-bulb temperatures or heat indices, are measured in different conditions and account for different weather factors; the most appropriate for a given environment or outcome can vary within and across locations, and over time, making comparisons difficult. Accordingly, most large-scale studies employ satellite-based land surface temperatures to facilitate the study of urban heating both within and across geographies. Although these measurements are not equivalent to the standard heat exposure metrics, they are statistically related to near-surface air temperatures

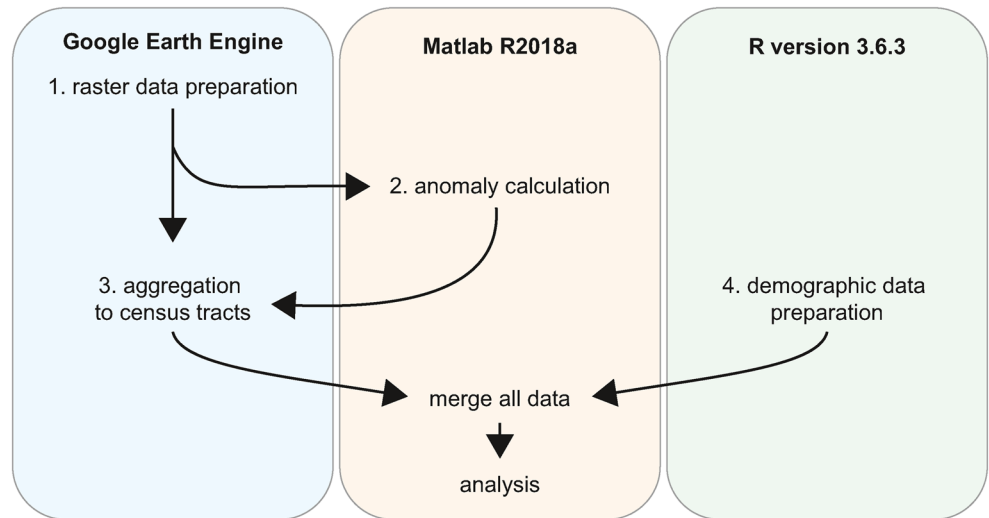


**Figure 1.** Flowchart describing the overall layout of data acquisition.

(Benz, Bayer, & Blum, 2017; Mostovoy et al., 2006) and provide near-uniform coverage over large regions. Importantly, they therefore allow for systematic exploration of whether—despite very different agro-ecologies, social and political histories, and physical geographies—local patterns of environmental injustice in urban heat exposure hold more broadly. Urban climate studies based on land surface temperatures in several (primarily US) cities have revealed that these within-city gradients are often strongly correlated with neighborhood socioeconomic characteristics, with low-income areas and neighborhoods with larger racial minority population shares exposed to higher average and extreme temperatures (Chakraborty et al., 2019, 2020; Hoffman et al., 2020; Hsu et al., 2021; Mitchell & Chakraborty, 2014).

To date, however, explorations of disparities over larger spatial scales have been limited to major urban hubs, disregarding smaller settlements. In addition, we have little knowledge on how heat disparities scale with the heterogeneity and diversity of local populations, if there are regional patterns in their drivers, and we do not know how they develop over time. Here, we quantify surface urban heat anomalies ( $\Delta T$ )—the difference in extreme summer surface temperatures in urban areas compared to their rural surroundings—for all developed lands within the contiguous United States at the 1-km resolution (2010–2014). We aggregate these surface temperature anomalies to the census tract level and match them with socioeconomic and demographic data from the American Community Survey (ACS) to analyze the distributions of urban heat extremes within and across the 1,056 counties that have at least 10 built-up census tracts. This sample includes both large cities and small towns, and covers more than 300 million people. We test whether and how much urban heat varies within localities on average, and how much of the unadjusted relationships between racial and ethnic neighborhood composition and temperature anomalies can be explained by income. We exploit land surface temperature data to understand how features of urban design—vegetation, built-up area, albedo and population density—contribute to remaining race- and class-based disparities, and further explore whether and how these patterns have changed in the past decade.

## 2. Data Pre-Processing

### 2.1. Overview

This study combines raster imagery (primarily satellite-based) with demographic variables at the census tract level. Data was (primarily) prepared using Google Earth Engine (Gorelick et al., 2017), Matlab R2018a, and the R programming environment. Processing of data consists of four distinct steps (see flowchart in Figure 1): (a) raster data preparation, (b) anomaly calculation, (c) aggregation to census tracts, and (d) demographic data preparation. Then all data are merged and we begin the analysis.

## 2.2. Raster Data Preparation

### 2.2.1. Methodology

Data in the raster format was pre-processed in Google Earth Engine (GEE) (Gorelick et al., 2017). Specifics are listed below for all individual data products. All of them were prepared in a resolution of approximately  $1 \times 1$  km ( $0.009^\circ \times 0.009^\circ$ )—the native resolution of the land surface temperature product.

### 2.2.2. Land Surface Temperatures

While urban climate literature has focused on urban canopy temperatures (and more specifically wet-bulb temperature) as the most relevant metrics for potentially dangerous human heat exposure, such temperatures are only available via ground-based weather stations. This facilitates local study, but precludes large-scale analysis. In contrast, satellite-based daily land surface temperatures (LST) are available for the entire US at a 1-km resolution. While surface temperatures are not equivalent to air temperatures, both vary in accordance with surface energy balance parameters. LST thus enable understanding of differential exposures, even if they do not perfectly correlate with (e.g.,) established extreme heat thresholds.

For this study we analyze summertime land surface temperatures (LSTs) between June 1 and August 31 for the 5 years 2010–2014 (and later also 2005–2009 and 2015–2019). Data are collected for daytime and nighttime separately from the daily MODIS V6 LST products MOD11A1 (Z. Wan, 2015a) and MYD11A1 (Z. Wan, 2015b). Data are available for cloud free, land pixels only, additionally we filter out all data with an error  $\geq 2$  K.

Our main analysis focuses on the 95th percentile of temperatures as a measure of extreme summer temperatures, but supplement analysis includes assessments of mean temperatures as well as studying morning (MOD11A1) and afternoon (MYD11A1) imagery separately.

### 2.2.3. Nighttime Lights

Five-year mean (2010–2014) nighttime lights were compiled from Version 4 of the DMSP-OLS Nighttime Lights Time Series, Image and Data processing by NOAA's National Geophysical Data Center, and DMSP data collection by the US Air Force Weather Agency. They are expressed as digital numbers (DN) ranging from 0 to 63.

### 2.2.4. Elevation and Aspect

For elevation we rely on the Global Multi-resolution Terrain Elevation Data 2010 courtesy of the US Geological Survey (Danielson & Gesch, 2011). Aspect data were generated from these using ArcGIS Version 10.5.

### 2.2.5. Normalized Difference Built-Up Index

The Normalized Difference Built-up Index (NDBI) is defined as the normalized difference between Short-wave Infrared (SWIR) and Near Infrared (NIR) bands and intended to map built-up areas (Zha et al., 2003).

$$NDBI = \frac{SWIR - NIR}{SWIR + NIR} \quad (1)$$

Here we determine NDBI for the MODIS product MYD09A1 V6 (E. Vermote, 2015) using bands 7 and 2 for all cloud free pixels for all images in the assessed time frame before determining the 5-year mean (2010–2014, and later also 2005–2009 and 2015–2019).

### 2.2.6. Normalized Difference Vegetation Index

Normalized Difference Vegetation Index (NDVI) is prepared as the 5-year mean (2010–2014, and later also 2005–2009 and 2015–2019) of combined MODIS products MOD13A2 (K. Didan, 2015a) and MYD13A2 (K. Didan, 2015b).

### 2.2.7. Black-Sky Albedo

Black-sky albedo (BSA) is prepared as the 5-year mean (2010–2014, and later also 2005–2009 and 2015–2019) of MODIS product MCD43C3: BSA for shortwave broadband (C. Schaaf, 2015).

### 2.2.8. Land Cover

To identify developed areas we used the USGS National Land Cover Database 2013 (L. Yang et al., 2018) and its classes developed open space, developed low intensity, developed medium intensity, and developed high intensity. While this data set has a native resolution of 30 m, we exported it from GEE in a 1 km resolution to match all other data. To do so GEE internally runs two processing steps: first it accesses the pyramid level closest to the specified resolution—pyramiding policy for discrete valued images is sampling the top left pixel at the next lower level. Then nearest neighbor resampling is employed to reach the specified resolution.

## 2.3. Anomaly Calculation

### 2.3.1. Surface Urban Heat Anomalies

Surface urban heat anomalies  $\Delta T$  are determined for all pixels classified as developed lands within the contiguous United States. For a pixel  $ij$ , they are defined as the difference in local LST and rural background LST (Benz, Bayer, & Blum, 2017; Benz, Davis, & Burney, 2021):

$$\Delta T_{ij} = T_{ij} - \text{median}(T_{\text{rural}})_{ij} \quad (2)$$

In contrast to LST, they do not convey large-scale climate regimes, instead they primarily display the impact of urban land cover changes on the local surface energy balance. They therefore might be the more appropriate tool to test how our policies and urbanization strategies have actively shaped heat disparities.

We define the rural background of pixel  $ij$ , as all pixels that are

- within 100 pixels ( $\approx 100$  km) of pixel  $ij$
- are elevated  $\pm 100$  m compared to pixel  $ij$
- have an aspect of  $\pm 90^\circ$  compared to pixel  $ij$
- and have a nighttime light  $\leq \text{DN}15$ .

This is in line with previous studies using this method, please refer to Benz, Davis, and Burney (2021) for an in depth description and a sensitivity analysis.

### 2.3.2. NDBI, NDVI, and BSA Anomalies

NDBI, NDVI, and BSA were process the same way as surface temperatures anomalies in order to express the difference in urban and rural parameters following Equation 2.

$$\Delta \text{NDBI}_{ij} = \text{NDBI}_{ij} - \text{median}(\text{NDBI}_{\text{rural}})_{ij} \quad (3)$$

$$\Delta \text{NDVI}_{ij} = \text{NDVI}_{ij} - \text{median}(\text{NDVI}_{\text{rural}})_{ij} \quad (4)$$

$$\Delta \text{BSA}_{ij} = \text{NDBI}_{ij} - \text{median}(\text{BSA}_{\text{rural}})_{ij} \quad (5)$$

It is important to note that all of these parameters are correlated (see Table S1) and therefore not fully independent.

## 2.4. Aggregation to Census Tracts

Mean  $\Delta T$  (based on 95th percentile summer daytime and nighttime LST, on mean summer daytime and nighttime LST and for morning and afternoon),  $\Delta \text{NDBI}$ ,  $\Delta \text{NDVI}$ ,  $\Delta \text{BSA}$ , LST (95th percentile summer daytime and nighttime temperatures), and the number of observations (for LST) are determined for each census tract in the contiguous US. This was performed at a resolution of 100 m in GEE. Based on the internal scaling algorithm of GEE this effectively weights each 1 km pixel based on their area inside each census tract. Because  $\Delta T$  was only determined for pixels classified as developed lands, mean values can only be determined for census tract with with developed lands in them—in the following these 70,901 census tracts are referred to as developed census tracts.

### 2.5. Demographic Data Preparation

To identify affected populations we extracted data from the US Census Bureau 2014 5-year American Community Survey (ACS) for all census tracts in the contiguous US using the *tidycensus* package (Walker, 2020) for the R programming environment. We extracted the following nine demographic variables:

- *Share Black* defined as the share of individuals identifying as Black or African Americans alone or in combination with one or more other races. This variable was also extracted for the 2009 and 2019 5-year ACS.
- *Share non-Hispanic White* defined as the share of individuals identifying as White but not ethnically Hispanic or Latinx.
- *Share Hispanic* (We do not filter for overlaps in share Hispanic and share Black or Asian). This variable was also extracted for the 2009 and 2019 5-year ACS.
- *Share Asian* defined as the share of individuals identifying as Asian and no other race. This variable was also extracted for the 2009 and 2019 5-year ACS.
- *Share non-US citizens*.
- *Share with high school diploma or less* which includes High school equivalency.
- *Share kids with single parents* describes the share of children under the age of 18 living with one parent.
- *Share 75 years or older*.
- *Median income* in the past 12 month in 2014 inflation-adjusted US\$.

In addition the total population count (following the 2009, 2014, and 2019 5-year ACS) was divided by the tract area to get population density.

## 3. Results

### 3.1. Surface Urban Heat Extremes in the US

To understand how population and  $\Delta T$  distributions are related, we aggregate  $\Delta T$  to the census tract level and link these measurements with socioeconomic and demographic data (Figure 2). We find that 78% of all census tracts, housing 79% of the population in our study area, have surface urban heating during daytime (Figure S1). Daytime surface urban cooling is found in the semi-arid region of the Sunbelt and Rocky Mountains, with Phoenix highlighted as an example in Figure 2d. Beyond these regional patterns,  $\Delta T$  is linked to urban design parameters: at daytime  $\Delta NDBI$  and  $\Delta NDVI$  show the strongest correlation to  $\Delta T$  but those reduce notably during nighttime. At night, population density (at the log scale), NDVI and  $\Delta BSA$  show the highest correlations (Figure S2). Importantly, our statistical analysis of BSA add dimension to the current understanding of albedo—existing more physics-constrained approaches found a moderate increase in albedo drives daytime surface cooling and has no effect at night in selected cities in the southern United States (Zhao et al., 2014).

To assess how this surface urban heat burden is distributed, we divide census tracts within each county into income (and other demographic) quartiles. As an illustration of this methodology, average daytime and nighttime  $\Delta T$  by income for five selected counties are shown in Figure 2: in each of these areas, the first quartile (representing the poorest census tracts in the county) has more intense surface temperature anomalies than the fourth quartile (richest) census tracts. Across these cases,  $\Delta T$  and surface urban heat disparities are more extreme during daytime than nighttime. Even in Phoenix, where we find surface urban cooling during daytime, the cooling is less pronounced for poorer communities, meaning they experience relatively higher surface temperatures compared to their wealthier neighbors. There is some city-specific as well as regional-scale heterogeneity: Miami-Dade has no discernible nighttime effect, but the daytime income disparity is pronounced. Additionally, rank-ordering of surface heat by income quartile is non-uniform across these sites: in Seattle nighttime  $\Delta T$  is decreasing from fourth to third to second quartile and then up again for the poorest quartile. Similarly daytime  $\Delta T$  in Brooklyn is higher for the third and second quartiles than the first. We find similar patterns for other demographic gradients within counties: census tracts with higher shares of Black, Hispanic, Asian, and lower education levels have higher urban surface temperature anomalies Figure S3.

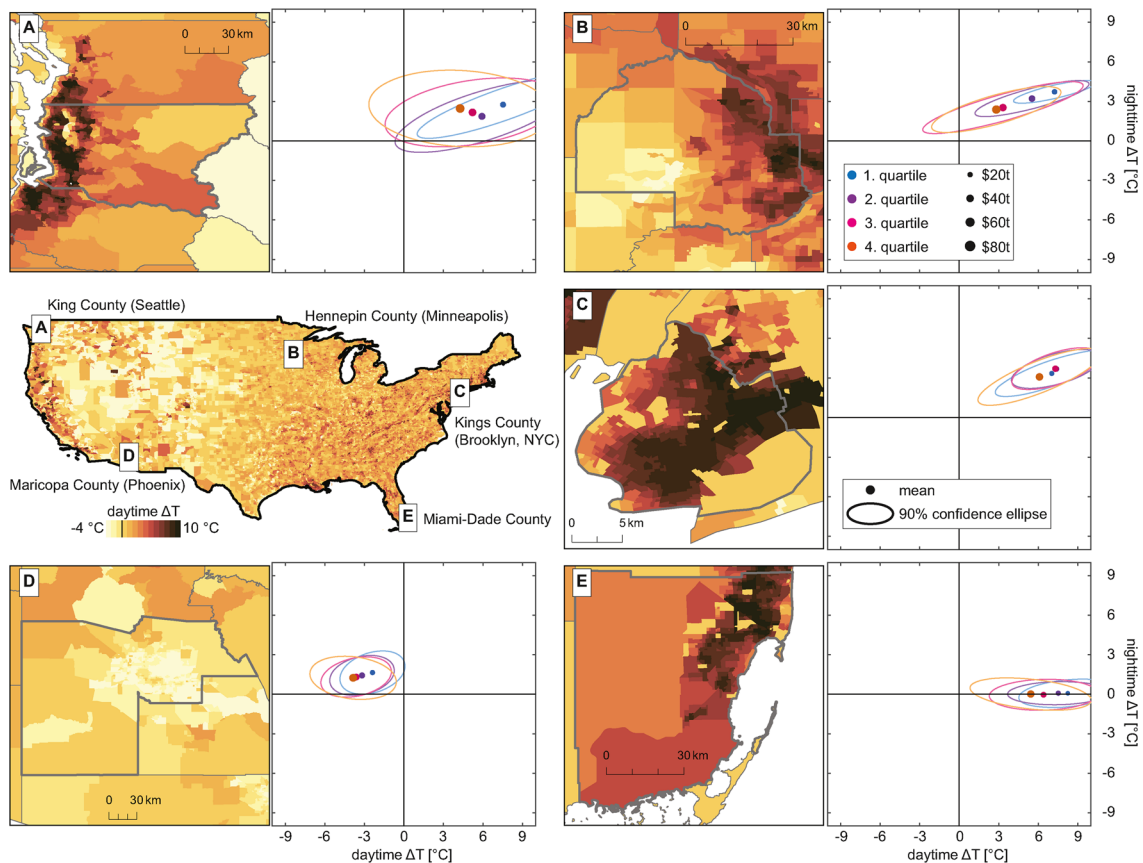


**Figure 2.** Maps of extreme summer daytime surface urban heat  $\Delta T$  within the US and selected counties. Shown is average  $\Delta T$  of all developed areas within a census tract. Inset areas show the heterogeneity within urban areas (Selected counties are A: King County, Washington (Seattle); B: Hennepin County, Minnesota (Minneapolis); C: Kings County, New York (Brooklyn, NYC); D: Maricopa County, Arizona (Phoenix); and E: Miami-Dade County, Florida.) For each inset, the corresponding dot-and-ellipse plots show the distributions of daytime and nighttime  $\Delta T$  by income quartiles, with dots showing the quartile mean for all census tracts within that county. The size of the dot shows the mean income of the corresponding quartile, since income distributions vary across the country.

### 3.2. Widespread Inequality in Heat Distributions

We extend this analysis to include all 1,056 counties that contain at least 10 developed census tracts, and examined the distribution of surface urban heat anomalies across a range of socioeconomic and demographic gradients (these results can be visualized in a Google Earth Engine app accessible at <https://sabenzenz.users.earthengine.app/view/urbanheatusa>).

The summary across all analyzed counties is visualized in Figure 3, where each point represents the difference in  $\Delta T$  for the county between the first and last quartile for the specified indicator. Point size corresponds to the number of census tracts contained in the county, and color provides an indication of overall demographic heterogeneity (here quantified as the interquartile range—IQR). In addition, we show the distribution of daytime  $\Delta T$  by counties with low versus high IQR underneath each panel. A few noteworthy patterns emerge from these raw distributions: First, on average, surface daytime urban heat disparities are much larger than nighttime disparities. Second, the racial, ethnic, and US-origin-based disparities are pronounced: 77% of all counties show significant daytime  $\Delta T$  differences between census tracts with the highest and lowest Black population shares. Similarly, for 81% of these counties the most non-Hispanic White tracts have significantly lower daytime  $\Delta T$  than their Hispanic and/or non-White neighbors. These numbers change slightly when considering only Hispanic ethnicity: 71% of counties have significantly higher urban surface temperatures in the census tracts with the highest Hispanic population shares compared to the lowest. These patterns extend beyond race and ethnicity: 72% of counties have such disparities for neighborhoods with high versus low shares of non-US citizens, 77% for neighborhoods with high versus low

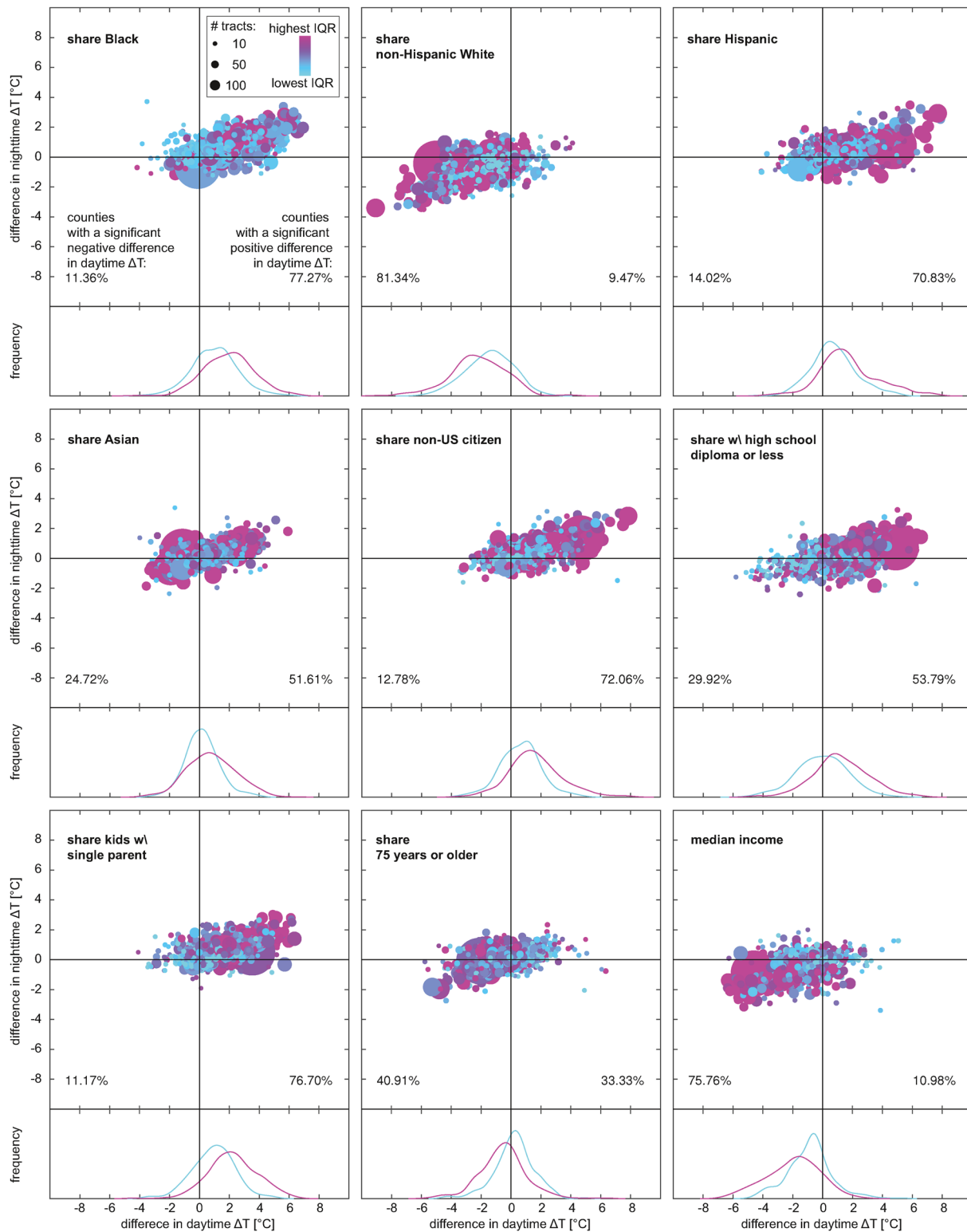


**Figure 3.** Difference in daytime and nighttime  $\Delta T$  for highest and lowest quartiles of nine demographic variables for all 1,056 counties analyzed in this study. Each dot represents the difference in first and last quartile of a county for the corresponding demographic variable. The size of the county as its number of developed census tracts. The color gives information on the interquartile range (IQR) of the demographic variable in each county. The histograms below each plot show the distribution of counties with the lowest (blue) and highest (magenta) 25% of IQRs. Percentages in the corners gives percentage of counties with significant differences in daytime  $\Delta T$  for each side.

shares of single-parent households, and 76% show significant differences between the poorest and richest census tracts.

These patterns are similar, but borne out to a lesser degree across a number of other social and demographic indicators. In 52% of counties, census tracts with the highest Asian population shares have significantly more surface urban heat than areas with low Asian population shares, but in 25% of counties the opposite is true. For education level there is a similar divide, with 54% of counties having significantly higher  $\Delta T$  for lower education levels, but 30% the other way. There is also no evidence of average age-based disparities across counties, which is particularly relevant as the elderly are more susceptible to heat related mortality (Anderson & Bell, 2009). These disparities are also present in absolute LST (instead of  $\Delta T$ , Figure S4), in  $\Delta T$  based on morning and afternoon surface temperatures (Figure S5), and in  $\Delta T$  based on summer-mean surface temperatures (instead of summer extremes, Figure S6).

We also see evidence of nonlinearity in unequal extreme surface heat exposures. We find that more homogeneous counties—as quantified by a smaller interquartile range (IQR) of a given social, economic, or demographic indicator—have smaller surface urban heat disparities than more heterogeneous counties. These distributional differences are shown in the histograms underneath each panel in Figure 3. However, average disparities do not disappear for more homogeneous counties, except in the cases of Asian population share, education level, and age. For other indicators, while the disparities are less extreme, unequal surface urban heat distribution is nevertheless still significant for the majority of racial and economic demographic variables. For income-based surface temperature disparities we observe that a tenfold increase in IQR amplifies disparities by 2.0°C (Figure S7a). We also find evidence that counties with higher overall populations have higher surface temperature disparities across the income gradient (Figure S7b). This can be partially attributed to the fact that  $\Delta T$  scales with population density (Figure S2). However, since even much less densely populated counties show significant differences in surface urban heating, this indicates that urban design parameters are major drivers across urban areas of different sizes. Regional patterns of class-based surface heat disparities are displayed in Figure S8a. At the county level, average differences in daytime  $\Delta T$  between richest and poorest census tracts are highest in the Northeast.

### 3.3. Controlling for Income

While Figure 3 shows raw racial, ethnic, and class-based surface urban heat disparities, a key policy question is the extent to which racial and ethnic surface urban heat disparities are explained by income. We test for the existence of race, ethnicity, and class-based disparities *beyond* income-driven effects by first establishing a linear regression relationship for surface urban heat and income for each county, and then analyzing whether the  $\Delta T$  residuals are still correlated with demographics. These results are shown in Figure 4.

We find that, even when controlling for income, 71% of all counties have significantly lower  $\Delta T$  for predominantly non-Hispanic White communities than less White or more Hispanic neighborhoods. The magnitudes are smaller, but statistically significant disparities persist after adjusting for income for Black (with 65% of counties showing significant differences), Hispanic (61%), and Asian (57%) population shares. Similarly non-US citizens live in areas of higher  $\Delta T$  for 64% of all counties. We still see no evidence of disparities based on age, although education and single-parent household disparities remain. Interestingly, controlling for income removes much of the nonlinearity: the larger impacts in more heterogeneous counties visible in Figure 3 are dramatically reduced (Figure 4, histograms). Notable exceptions are for education and Asian population share where surface heat disparity is only skewed for counties with higher IQR. The latter may be driven by relatively low Asian population shares in the US compared to Hispanic and Black populations (5% compared to 17% or 14%), and their distributions: 55% of counties have less than 1% share Asian. Asian population share is also the one variable for which significant differences in  $\Delta T$  increases after controlling for income. This may be due to a very heterogeneous income distribution across the diverse Asian communities of the United States (for example, one study focusing on surface urban heat in Pinellas county, Florida e.g., identified specifically Southeast Asian communities being primarily exposed to surface urban heat [Mitchell & Chakraborty, 2014]). Controlling for income does not dramatically change the regional pattern of  $\Delta T$  disparities (Figure S8b).



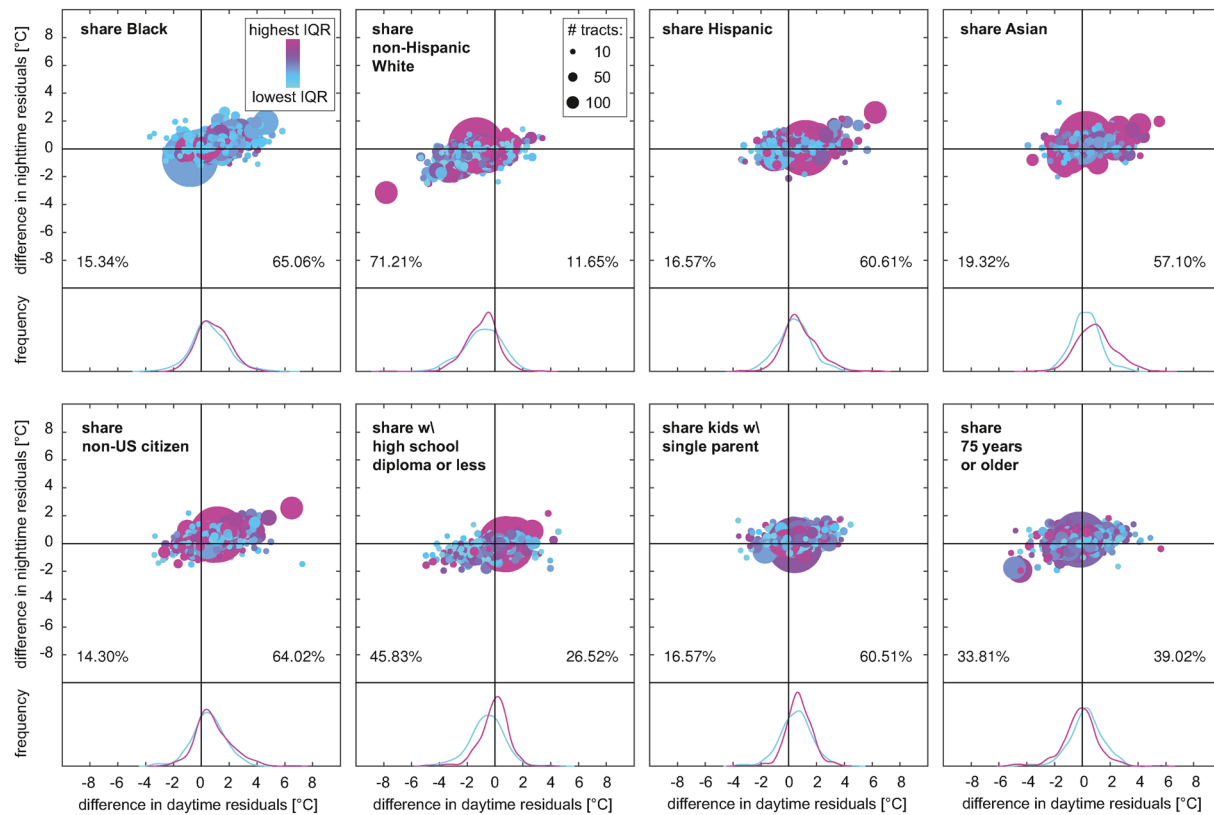


**Figure 4.** Difference in daytime and nighttime  $\Delta T$  residuals for highest and lowest quartiles of eight demographic variables for all 1,056 counties analyzed in this study, after controlling for income. Each dot represents the difference in first and last quartile of a county for the corresponding demographic variable. The size of the dot represents the size of the county as its number of developed census tracts. The color gives information on the interquartile range (IQR) of the demographic variable in each county. The histograms below each plot show the distribution of counties with the lowest (blue) and highest (magenta) 25% of IQRs. Percentages in the corners gives percentage of counties with significant differences in daytime  $\Delta T$  residuals for each side.

### 3.4. The Impact of Urban Design

On a physical level, surface urban heat anomalies are driven by alterations of the surface energy balance that are a function of urban design. While many types of policies and labor market conditions contribute to the human geography of neighborhoods, we explore whether there are commonalities in the physical drivers of surface urban heat disparities by using satellite-based observations of key contributors. Among the parameters altering the surface energy balance are heavily built-up areas that trap radiation (here measured as  $\Delta NDBI$ ), the existence of vegetation, which can cool the surface through evapotranspiration (here  $\Delta NDVI$ ), the potential of the surface to absorb—and later release—heat (here expressed as  $\Delta BSA$ ), and our waste heat (here measured as population density). As described above, each of these affects surface urban heating in a measurable way, particularly during the daytime when  $\Delta NDBI$  and  $\Delta NDVI$  appear to be main drivers (Figure S2). Here, we assess the extent to which they are correlated with the observed surface heat exposure disparities. Again, to separate income from other race- and class-based disparities, we control for income by determining the residuals from a linear regression between median income and  $\Delta NDBI$ ,  $\Delta NDVI$ ,  $\Delta BSA$ , and population density, respectively. Analyzing the differences between the first and fourth quartiles of selected demographic variables in each county we are able to visualize the difference in urban design factors driving these disparities (Figure 5).

We observe notable differences between the richest and poorest census tracts in population density,  $\Delta NDBI$ , and  $\Delta NDVI$  but no difference in  $\Delta BSA$ . The mean highest-income quartile has a 0.07 higher  $\Delta NDVI$  than the mean lowest-income quartile—in comparison a study of 102 urban US areas in 2010 found a difference in  $\Delta NDVI$  of 0.11 between the best (Grade A) and lowest (redlined) graded neighborhoods (Nardone et al., 2021). We observe similar differences in these urban design parameters—after controlling for

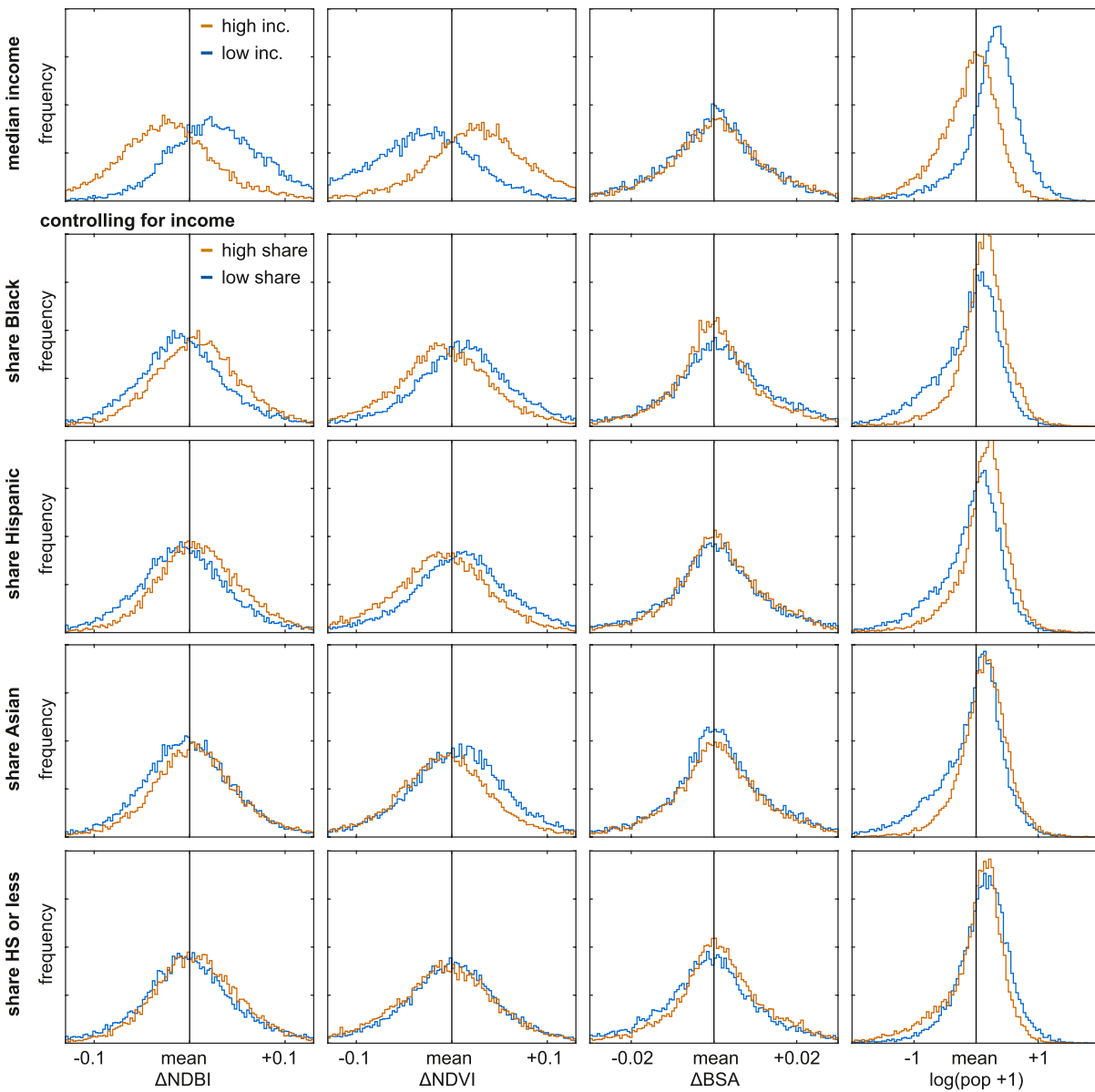


**Figure 5.** Effects of urban design parameters on daytime and nighttime  $\Delta T$  and their distribution for lowest and highest quartile of income and selected demographic variables after controlling for income. Shown are deviation from county average for built-up index (NDBI), vegetation index (NDVI), albedo (BSA), and population density (at the log scale).

income—for Black, Hispanic, and Asian population shares. High non-White or Hispanic share census tracts show slightly higher population density, higher  $\Delta NDBI$ , and lower  $\Delta NDVI$ . (For Asian population share, the distribution of  $\Delta T$  is quite skewed—in many counties more than 25% of the tracts have no Asian population at all resulting in more tracts being represented in the first quartile than in the last). We find no notable differences in  $\Delta NDBI$  and  $\Delta NDVI$  based on education level—the observed differences in surface urban heat appear to be primarily linked to population densities, with lower education communities living at higher densities.

### 3.5. Temporal Development

Another question is how these surface urban heat disparities have developed over the last decade. We compare  $\Delta T$  for the 5 years before and after the results reported above (2005–2009 and 2015–2019) but keep the

demographics from 2010 to 2014 (as most variables are not available for the 2005–2009 time period). Still, we are able to quantify migration for Share Black, Hispanic and Asian and find only little movement (Figure S9). Analyzing the change in disparities in  $\Delta T$  between these years we find no clear countrywide trend (Figure S10). On average (median of all counties) we find changes in disparities of less than  $0.1^\circ\text{C}$  for all our demographic variables and cannot identify a significant, widespread movement in either direction. However, this obscures the fact that there is a wide variance. Roughly 10% of counties (106 counties) saw increased class-based disparities of more than  $0.5^\circ\text{C}$  compared to 75 counties where disparities decreased by more than  $0.5^\circ\text{C}$  (Figure S10). Comparing these two groups we find that counties with increasing class disparities increased vegetation ( $\Delta\text{NDVI}$ ) more in wealthier census tracts. Counties with decreasing class disparities on the other hand show increased  $\Delta\text{NDVI}$  for poorer neighborhoods and at the same time increased  $\Delta\text{NDBI}$  in wealthier tracts. Both groups show a higher increase in BSA for low-income communities (Figure S11). There are no notable migration patterns in either group (Figure S9).

#### 4. Discussion

Roughly 25% of all natural hazard mortality in the United States is due to heat exposure (Borden & Cutter, 2008) and heat waves are becoming more frequent, more intense, and are longer in season (Shiva et al., 2019; Wobus et al., 2018); understanding who is affected by urban heating and what drives exposure disparities is therefore critical for crafting just and effective policy responses, particularly under warming climate conditions. Here we use Land Surface Temperature (LST) data to understand patterns of surface urban heat disparities, and to compare them within more than 1,000 counties across the continental US. We find that 75% of all counties (housing 84% of the population) have significant more daytime urban warming in lower-income census tracts. This variation is also associated with the racial and ethnic composition of neighborhoods, an effect that persists even when controlling for income (71% of counties, housing 76% of the represented population, have statistically significant race disparities after adjusting for income). Additionally, while the composition and history of communities varies across the country (e.g., the southeast vs. southwest), these disparities are starkly consistent over this vast region, and on a physical level look very similar: they are driven by high population densities, more built-up areas, and less vegetation in the most affected communities.

Our findings broadly agree with earlier literature: a recent study focusing on 25 cities around the world showed that 72% have an income gradient in which poorer neighborhoods experience more surface urban heat (Chakraborty et al., 2019); another study found that in 88% of US cities surface urban heat correlates negatively with income (Chakraborty et al., 2020); and yet another study on 175 urban areas in the US found that in over 70% of those people with an income below the poverty line have a significantly higher exposure than people with an income above twice the poverty line (Hsu et al., 2021). An important contribution of the analyses presented here is the finding that these racial and ethnic inequalities are present even in more rural counties; such smaller urban areas are often excluded from urban heating studies. The existence of these gradients implies that the inequality we find in our cities does not only develop after large urbanization and growth, but manifests early in the existence of a city itself. Hence, if fixing the root causes of urban heat disparities for future cities is an objective, policymakers will need to be much more proactive in smaller areas.

While the findings presented here are robust, the analysis nevertheless requires several caveats. First, while land surface temperatures are not the temperatures experienced by urban inhabitants, they are strongly correlated with air temperatures and are therefore a good proxy for actual exposures. Second, we compare summer extremes, but the seasonality of urban heat is dependent on water availability, meaning that maximal differences in urban versus rural extremes could present in different seasons (Manoli et al., 2020).

It is also important to note that LST and  $\Delta T$  are based on a different number of observations for different locations showing large-scale spatial patterns based on cloud coverage (Figure S12). We also find a distinct correlation between data availability and the demographics analyzed in this study—in disadvantaged communities there is less data available even within the same county (Figure S13). We hypothesize that this is caused by more smog (making atmospheric correction more difficult) and more complex land covers (making estimating emissivity for more difficult). Because cloud cover occurs primarily on cold summer

days, it effectively shifts the 95th percentile temperatures towards clear-sky conditions. In contrast, images filtered based on high errors are not necessarily linked to climate conditions and hence do not shift 95th percentile temperatures. Accordingly, we test for a shift towards clear-sky temperatures and thus higher  $\Delta T$  for location with more cloud cover (not including any images filtered out because of their error): While there are patterns we see no clear trend when comparing income-based disparities of  $\Delta T$  and cloud cover (Figure S14).

We see some changes over time, but caution that these trends, while observable, cannot be interpreted as byproducts of deliberate policy choices. For example, a study focused on five cities that showed increases in urban greening in redlined districts found that this increase in greening was not part of formal policy but potentially due to economic downturn leading to abandonment and unintentional vegetation overgrowth (Field, 2020). In addition this study does not consider the effects of migration (due to a lack of temporal demographic, particularly income data) and covers only a short time period. We hope future studies can resolve these constraints and will be able to better quantify changes in class and race disparities in heat exposure in the US over time.

Importantly and relatedly, longer-run analyses over time, and linkages to more detailed labor market information are needed to better untangle present employment mechanisms that may drive these racial and ethnic disparities versus other policies (Zenou & Boccoard, 2000). Within the UK, residential sorting can be traced back as far as 1817 and is sustained long after initial drivers declined (Heblich et al., 2021). In the US, in particular the legacy of redlining looms large—previous studies have shown that among 108 cities with historic redlining, 94% have higher LST in the formally redlined areas. These areas have less tree canopy, more streets, and higher building densities, meaning that in addition to their other racist outcomes, redlining policies directly codified into law existing disparity in urban land use and reinforced urban design choices that magnify urban heating into the present (Hoffman et al., 2020).

A more detailed understanding of these layered policy drivers is needed to craft meaningful and lasting responses to mitigate urban heat disparities. From a physical perspective, the consistent human, building, and vegetation gradients that explain the local surface energy balance perturbations may imply simple technical solutions (e.g., put resources into greening the hottest neighborhoods [Wang et al., 2018]), but the interactions of race, ethnicity, and income in this study indicate the need to consider social and physical systems jointly. For example, studies have shown high willingness to pay to mitigate urban heat (Borzino et al., 2020), and so care must be taken to ensure that actions undertaken to mitigate urban heat disparities don't in fact accelerate gentrification (Haase et al., 2017). For example, Shokry et al. (2020) found a strong link between the development of green resilient infrastructure and decreasing minority populations in Philadelphia. The analyses presented here point to a need for coordinated activities over large-scales to address these disparities, in conjunction with holistic and forward-thinking urban planning that accounts for the impacts future urban changes will have on the surface energy balance.

## Data Availability Statement

All data is made available in the Harvard Dataverse in form of a spreadsheet at <https://doi.org/10.7910/DVN/1F72FB> (Burney, 2021). See supplement for a more detailed description.

## References

- Anderson, B. G., & Bell, M. L. (2009). Weather-related mortality. *Epidemiology*, 20(2), 205–213. <https://doi.org/10.1097/ede.0b013e318190ee08>
- Benz, S. A., Bayer, P., & Blum, P. (2017). Identifying anthropogenic anomalies in air, surface and groundwater temperatures in Germany. *Science of The Total Environment*, 584–585, 145–153. <https://doi.org/10.1016/j.scitotenv.2017.01.139>
- Benz, S. A., Davis, S. J., & Burney, J. A. (2021). Drivers and projections of global surface temperature anomalies at the local scale. *Environmental Research Letters*, 16, 064093. <https://doi.org/10.1088/1748-9326/ac0661>
- Borden, K. A., & Cutter, S. L. (2008). Spatial patterns of natural hazards mortality in the United States. *International Journal of Health Geographics*, 7(1), 64. <https://doi.org/10.1186/1476-072x-7-64>
- Borzino, N., Chng, S., Mughal, M. O., & Schubert, R. (2020). Willingness to pay for urban heat island mitigation: A case study of Singapore. *Climate*, 8(7), 82. <https://doi.org/10.3390/cli8070082>
- Burney, J. (2021). *Submission data for urban heat disparities project*. Harvard Dataverse. <https://doi.org/10.7910/DVN/1F72FB>
- Chakraborty, T., Hsu, A., Manya, D., & Sheriff, G. (2019). Disproportionately higher exposure to urban heat in lower-income neighborhoods: A multi-city perspective. *Environmental Research Letters*, 14(10), 105003. <https://doi.org/10.1088/1748-9326/ab3b99>

## Acknowledgments

S. A. Benz is supported by the Big Pixel Initiative at UC San Diego. J. A. Burney and S. A. Benz are supported by NSF/USDA NIFA INFEWS T1 #1619318. J. A. Burney is supported by NSF CNH-L #1715557. The authors would like to thank one anonymous reviewer and Jeremy S. Hoffman for their helpful comments.

- Chakraborty, T., Hsu, A., Many, D., & Sheriff, G. (2020). A spatially explicit surface urban heat island database for the United States: Characterization, uncertainties, and possible applications. *ISPRS Journal of Photogrammetry and Remote Sensing*, *168*, 74–88. <https://doi.org/10.1016/j.isprsjprs.2020.07.021>
- Danielson, J., & Gesch, D. (2011). *Global multi-resolution terrain elevation data 2010 (GMTED2010)* (No. 2011–1073). US Department of the Interior, US Geological Survey. <https://pubs.usgs.gov/of/2011/1073/pdf/of2011-1073.pdf>
- Didan, K. (2015a). *MOD13A2 MODIS/terra vegetation indices 16-day l3 global 1 km SIN grid v006*. NASA EOSDIS Land Processes DAAC. Retrieved from <https://lpdaac.usgs.gov/products/mod13a2v006/>
- Didan, K. (2015b). *MYD13A2 MODIS/aqua vegetation indices 16-day l3 global 1 km SIN grid v006*. NASA EOSDIS Land Processes DAAC. Retrieved from <https://lpdaac.usgs.gov/products/myd13a2v006/>
- Field, J. M. (2020). *Urban tree canopy governance and redlined neighborhoods: An analysis of five cities* (Master's thesis). Massachusetts Institute of Technology. Retrieved from <https://hdl.handle.net/1721.1/127588>
- Gorelick, N., Hancher, M., Dixon, M., Ilyushchenko, S., Thau, D., & Moore, R. (2017). Google Earth Engine: Planetary-scale geospatial analysis for everyone. *Remote Sensing of Environment*, *202*, 18–27. <https://doi.org/10.1016/j.rse.2017.06.031>
- Grimmond, S. (2007). Urbanization and global environmental change: Local effects of urban warming. *The Geographical Journal*, *173*(1), 83–88. [https://doi.org/10.1111/j.1475-4959.2007.232\\_3.x](https://doi.org/10.1111/j.1475-4959.2007.232_3.x)
- Haase, D., Kabisch, S., Haase, A., Andersson, E., Banzhaf, E., Baró, F., et al. (2017). Greening cities – To be socially inclusive? About the alleged paradox of society and ecology in cities. *Habitat International*, *64*, 41–48. <https://doi.org/10.1016/j.habitatint.2017.04.005>
- Heblisch, S., Trew, A., & Zylberberg, Y. (2021). East-side story: Historical pollution and persistent neighborhood sorting. *Journal of Political Economy*, *129*, 1508–1552. <https://doi.org/10.1086/713101>
- Hoffman, J. S., Shandas, V., & Pendleton, N. (2020). The effects of historical housing policies on resident exposure to intra-urban heat: A study of 108 US urban areas. *Climate*, *8*(1), 12. <https://doi.org/10.3390/cli8010012>
- Hsiang, S. M., Burke, M., & Miguel, E. (2013). Quantifying the influence of climate on human conflict. *Science*, *341*(6151), 1235367. <https://doi.org/10.1126/science.1235367>
- Hsu, A., Sheriff, G., Chakraborty, T., & Many, D. (2021). Disproportionate exposure to urban heat island intensity across major US cities. *Nature Communications*, *12*(1). <https://doi.org/10.1038/s41467-021-22799-5>
- Laaidi, K., Zeghnoun, A., Dousset, B., Bretin, P., Vandentorren, S., Giraudet, E., & Beaudou, P. (2012). The impact of heat islands on mortality in Paris during the August 2003 heat wave. *Environmental Health Perspectives*, *120*(2), 254–259. <https://doi.org/10.1289/ehp.1103532>
- Manoli, G., Fatichi, S., Bou-Zeid, E., & Katul, G. G. (2020). Seasonal hysteresis of surface urban heat islands. *Proceedings of the National Academy of Sciences*, *117*(13), 7082–7089. <https://doi.org/10.1073/pnas.1917554117>
- Mitchell, B. C., & Chakraborty, J. (2014). Urban heat and climate justice: A landscape of thermal inequity in Pinellas County, Florida. *Geographical Review*, *104*(4), 459–480. <https://doi.org/10.1111/j.1931-0846.2014.12039.x>
- Mostovoy, G. V., King, R. L., Reddy, K. R., Kakani, V. G., & Filippova, M. G. (2006). Statistical estimation of daily maximum and minimum air temperatures from MODIS LST data over the state of Mississippi. *GIScience & Remote Sensing*, *43*(1), 78–110. <https://doi.org/10.2747/1548-1603.43.1.78>
- Nardone, A., Rudolph, K. E., Morello-Frosch, R., & Casey, J. A. (2021). Redlines and greenspace: The relationship between historical redlining and 2010 greenspace across the United States. *Environmental Health Perspectives*, *129*(1), 017006. <https://doi.org/10.1289/ehp7495>
- Pyrgou, A., & Santamouris, M. (2018). Increasing probability of heat-related mortality in a Mediterranean city due to urban warming. *International Journal of Environmental Research and Public Health*, *15*(8), 1571. <https://doi.org/10.3390/ijerph15081571>
- Ridder, K. D., Maiheu, B., Lauwaet, D., Daglis, I., Keramitsoglou, I., Kourtidis, K., et al. (2016). Urban heat island intensification during hot spells—The case of Paris during the summer of 2003. *Urban Science*, *1*(1), 3. <https://doi.org/10.3390/urbansci1010003>
- Schaaf, C. (2015). *MCD43A3 MODIS/terra+ aqua BRDF/albedo daily L3 global - 500 m v006*. NASA EOSDIS Land Processes DAAC. Retrieved from <https://lpdaac.usgs.gov/products/mcd43a3v006/>
- Shiva, J. S., Chandler, D. G., & Kunkel, K. E. (2019). Localized changes in heat wave properties across the United States. *Earth's Future*, *7*(3), 300–319. <https://doi.org/10.1029/2018ef001085>
- Shokry, G., Connolly, J. J., & Anguelovski, I. (2020). Understanding climate gentrification and shifting landscapes of protection and vulnerability in green resilient Philadelphia. *Urban Climate*, *31*, 100539. <https://doi.org/10.1016/j.uclim.2019.100539>
- Taylor, J., Wilkinson, P., Davies, M., Armstrong, B., Chalabi, Z., Mavrogianni, A., et al. (2015). Mapping the effects of urban heat island, housing, and age on excess heat-related mortality in London. *Urban Climate*, *14*, 517–528. <https://doi.org/10.1016/j.uclim.2015.08.001>
- Vermote, E. (2015). *MYD09A1 MODIS/aqua surface reflectance 8-day l3 global 500 m SIN grid v006*. NASA EOSDIS Land Processes DAAC. Retrieved from <https://lpdaac.usgs.gov/products/myd09a1v006/>
- Walker, K. (2020). *tidycensus: Load us census boundary and attribute data as 'tidyverse' and 'sf'-ready data frames [computer software manual]* (R package version 0.9.9.5). Retrieved from <https://CRAN.R-project.org/package=tidycensus>
- Wan, Z. (2015a). *MOD11A1 MODIS/terra land surface temperature/emissivity daily L3 global 1 km SIN grid v006*. NASA EOSDIS Land Processes DAAC. Retrieved from <https://lpdaac.usgs.gov/products/mod11a1v006/>
- Wan, Z. (2015b). *MYD11A1 MODIS/aqua land surface temperature/emissivity daily L3 global 1 km SIN grid v006*. NASA EOSDIS Land Processes DAAC. Retrieved from <https://lpdaac.usgs.gov/products/myd11a1v006/>
- Wang, C., Wang, Z.-H., & Yang, J. (2018). Cooling effect of urban trees on the built environment of contiguous United States. *Earth's Future*, *6*(8), 1066–1081. <https://doi.org/10.1029/2018ef000891>
- Whitman, S., Good, G., Donoghue, E. R., Benbow, N., Shou, W., & Mou, S. (1997). Mortality in Chicago attributed to the July 1995 heat wave. *American Journal of Public Health*, *87*(9), 1515–1518. <https://doi.org/10.2105/ajph.87.9.1515>
- Wobus, C., Zarakas, C., Malek, P., Sanderson, B., Crimmins, A., Kolian, M., et al. (2018). Reframing future risks of extreme heat in the United States. *Earth's Future*, *6*(9), 1323–1335. <https://doi.org/10.1029/2018ef000943>
- Yang, J., Yin, P., Sun, J., Wang, B., Zhou, M., Li, M., et al. (2019). Heatwave and mortality in 31 major Chinese cities: Definition, vulnerability and implications. *Science of The Total Environment*, *649*, 695–702. <https://doi.org/10.1016/j.scitotenv.2018.08.332>
- Yang, L., Jin, S., Danielson, P., Homer, C., Gass, L., Bender, S. M., et al. (2018). A new generation of the United States National Land Cover Database: Requirements, research priorities, design, and implementation strategies. *ISPRS Journal of Photogrammetry and Remote Sensing*, *146*, 108–123. <https://doi.org/10.1016/j.isprsjprs.2018.09.006>
- Zenou, Y., & Boccard, N. (2000). Racial discrimination and redlining in cities. *Journal of Urban Economics*, *48*(2), 260–285. <https://doi.org/10.1006/juec.1999.2166>

- Zha, Y., Gao, J., & Ni, S. (2003). Use of normalized difference built-up index in automatically mapping urban areas from TM imagery. *International Journal of Remote Sensing*, 24(3), 583–594. <https://doi.org/10.1080/01431160304987>
- Zhao, L., Lee, X., Smith, R. B., & Oleson, K. (2014). Strong contributions of local background climate to urban heat islands. *Nature*, 511(7508), 216–219. <https://doi.org/10.1038/nature13462>